

Research Article

Régis Straubhaar

Numerical Optimization of Eigenvalues of the Dirichlet–Laplace Operator on Domains in Surfaces

Abstract: Let (M, g) be a smooth and complete surface, $\Omega \subset M$ be a domain in M , and Δ_g be the Laplace operator on M . The spectrum of the Dirichlet–Laplace operator on Ω is a sequence $0 < \lambda_1(\Omega) \leq \lambda_2(\Omega) \leq \dots \nearrow \infty$. A classical question is to ask what is the domain Ω^* which minimizes $\lambda_m(\Omega)$ among all domains of a given area, and what is the value of the corresponding $\lambda_m(\Omega_m^*)$. The aim of this article is to present a numerical algorithm using shape optimization and based on the finite element method to find an approximation of a candidate for Ω_m^* . Some verifications with existing numerical results are carried out for the first eigenvalues of domains in \mathbb{R}^2 . Furthermore, some investigations are presented in the two-dimensional sphere to illustrate the case of the positive curvature, in hyperbolic space for the negative curvature and in a hyperboloid for a non-constant curvature.

Keywords: Spectral Geometry, Dirichlet–Laplace Operator, Eigenvalues, Numerical Approximations, Shape Optimization, Finite Element Method, Uzawa Algorithm

MSC 2010: Primary 65N25; secondary 49Q10, 35J05

Régis Straubhaar: Institut de Mathématiques, Université de Neuchâtel, Rue Emile-Argand 11, Case postale 158, 2009 Neuchâtel, Switzerland, e-mail: regis.straubhaar@unine.ch

1 Introduction

Let (M, g) be a smooth, complete Riemannian manifold of dimension 2 and $\Omega_M \subset M$ be a domain, namely a bounded open set in M . First, assume that $\partial\Omega_M$ is *regular enough*, for instance that $\partial\Omega_M$ is smooth. These assumptions on $\partial\Omega_M$ and g are weakened in the sequel. A Riemannian metric g being an inner product on each tangent space of the manifold, and so, it can be represented at each point x of M by a matrix $G(\pi(x)) \in \mathbb{M}_2(\mathbb{R})$ using a chart (U, π) , where $\Omega_M \subset U \subset M$ and $\pi : U \rightarrow \mathbb{R}^2$ is a diffeomorphism onto its range. Denote by x_1, x_2 the local coordinates and by Δ_g the Laplace operator given for all $f \in C^\infty(M)$ by

$$\Delta_g f = \frac{1}{\sqrt{\det(G)}} \sum_{j,k=1}^2 \partial x_j (G^{jk} \sqrt{\det(G)} \partial x_k f), \quad (1)$$

where G^{jk} is the (j, k) -component of the inverse of the matrix G . Consider the following underlying problem:

$$\begin{cases} \text{Find a map } u : \Omega_M \rightarrow \mathbb{R}, u \neq 0, \text{ and a scalar } \lambda \text{ such that} \\ -\Delta_g u = \lambda u \text{ in } \Omega_M \text{ and } u = 0 \text{ on } \partial\Omega_M. \end{cases} \quad (\mathcal{P})$$

The map u is called an *eigenfunction* associated to the *eigenvalue* λ . The spectral theorem for positive, self-adjoint and compact operators ensures that there exist a sequence $(u_m)_{m \in \mathbb{N} \setminus \{0\}}$ of eigenfunctions defining a Hilbert basis of $L^2(\Omega_M)$ and a sequence $(\lambda_m)_{m \in \mathbb{N} \setminus \{0\}}$ of associated eigenvalues such that

$$0 < \lambda_1 \leq \lambda_2 \leq \dots \nearrow \infty,$$

verifying $-\Delta_g u_m = \lambda_m u_m$ for all $m \in \mathbb{N} \setminus \{0\}$. In a sense to be specified in the next section, this remains true for the class of quasi-open sets. Using these notations, the optimization problem can be formulated as follows: for $m \in \mathbb{N} \setminus \{0\}$ and a certain fixed volume $0 < V < V_U$, where V_U is the volume of U :

$$\begin{cases} \text{Find a set } \Omega_m^* \subset M \text{ of volume } V \text{ such that the } m\text{-th eigenvalue } \lambda_m \text{ appearing} \\ \text{in problem } (\mathcal{P}) \text{ satisfies } \lambda_m(\Omega_m^*) \leq \lambda_m(\Omega) \text{ for all sets } \Omega \subset M \text{ of volume } V. \end{cases} \quad (\mathcal{P}_{\text{opt}})$$

Existence of optimal shapes in the class of quasi-open sets of \mathbb{R}^d , $d \in \mathbb{N}$, has been recently proved as a particular case in [7, 22]; see Remark 3.1 below. Moreover, it is shown that they are bounded and have finite perimeter. However, results giving explicit domains for this optimization problem exist only for $m = 1$ or 2 : in \mathbb{R}^2 , the inequality for the fixed membrane conjectured by Lord Rayleigh and independently proved by Faber and Krahn states that the domain minimizing λ_1 among all domains of fixed volume is a disc. The proof uses symmetrization techniques. This result also holds in the two-dimensional sphere and hyperbolic space. For $m = 2$ in \mathbb{R}^2 , the analogous result known as the Krahn–Szegő inequality asserts that the optimal domain Ω_2^* is the union of two identical discs. Unfortunately, the same arguments are ineffective for higher eigenvalues. See [5] for details and references on the topic.

The difficulty to find optimal shapes is the main reason to deal with it numerically. The precursory work [24] concerns domains in \mathbb{R}^2 with Dirichlet boundary conditions. It uses the finite element method and a descent algorithm to find optimal shapes. Other approaches also exist, for instance one based on the method of fundamental solutions [2, 3]. These latter works provide improvements and expand the problem to other boundary conditions as well as higher order eigenvalues optimization. Although numerical computations of eigenvalues on domains in surfaces already exist [19], no experimental works with regard to the optimization problem on surfaces are known to the author.

This paper is a first step towards the numerical optimization of eigenvalues on domains in surfaces. For this purpose, the approximation of eigenvalues is performed using a chart to carry out the computations in \mathbb{R}^2 endowed with a suitable metric. Some previous results [24] deal with domains in the euclidean space. Hence, the present work generalizes them to surfaces. To take the volume constraint into consideration in the shape optimization we use a Uzawa based method.

The paper is organized as follows. Section 2 is about the statement of the underlying problem (\mathcal{P}) and its formulation for the numerical computation of the eigenvalues. A study of the error made by approximating them is produced. Section 3 details the optimization algorithm, in particular the Uzawa based method for the shape optimization. Finally, in Section 4, some numerical results are presented. To check the validity of the program, the shapes obtained for the optimizers in \mathbb{R}^2 of the first fifteen eigenvalues are compared with theoretical results and with numerical computations from [2]. Furthermore, a verification is carried out for small domains in the sphere \mathbb{S}^2 and in the Poincaré disc \mathbb{D}^2 . At last, to illustrate various types of curvature, other examples in \mathbb{S}^2 , in \mathbb{D}^2 and in a hyperboloid are computed.

2 The Underlying Problem

2.1 Statement of the Underlying Problem

Let (M, g) be a smooth Riemannian manifold of dimension 2, $\Omega_M \subset M$ be a bounded open set in M , and (U, π) be a chart for M . For practical reasons, assume that $\Omega_M \subset U$ holds. Denote by Δ_g the Laplace operator given by (1) and consider the problem (\mathcal{P}) mentioned in the introduction.

For $k \in \mathbb{N} \setminus \{0\}$, let $H^k(\Omega_M)$ denote the Sobolev space of order k and $H_0^1(\Omega_M)$ the closure in $H^1(\Omega_M)$ of the space $C_0^\infty(\Omega_M)$ of $C^\infty(\Omega_M)$ -functions with compact support in Ω_M . A weak formulation of (\mathcal{P}) is

$$\left\{ \begin{array}{l} \text{Find } u \in H_0^1(\Omega_M), u \neq 0, \text{ and } \lambda \in \mathbb{R} \text{ such that} \\ \int_{\Omega_M} g(\nabla u, \nabla v) \, dV_g = \lambda \int_{\Omega_M} uv \, dV_g \text{ for all } v \in H_0^1(\Omega_M), \end{array} \right. \quad (\mathcal{WP})$$

where dV_g denotes the volume element on M and ∇ the gradient associated to g . The volume element dV_g can be written in terms of the Lebesgue measure using the local coordinates in $\pi(U)$ as $dV_g = \sqrt{\det G} \, dx_1 \, dx_2$. In the same way, the gradient of a function $v \in H_0^1(\Omega_M)$ is given by

$$\nabla v = G^{-1} \nabla_{\text{us}}(v \circ \pi),$$

where $\nabla_{\text{us}} = (\partial x_1, \partial x_2)$ denotes the usual gradient in \mathbb{R}^2 (in sense of the distribution theory). A solution u of (\mathcal{WP}) is called a *weak eigenfunction* and the associated λ is called a *weak eigenvalue*. Sometimes the dependence on the domain is emphasized by writing $u(\Omega_M)$ and $\lambda(\Omega_M)$.

The spectral theorem for positive, self-adjoint and compact operators ensures that there exist a sequence $(u_m)_{m \in \mathbb{N} \setminus \{0\}}$ of weak eigenfunctions defining a Hilbert basis of $L^2(\Omega_M)$ and a sequence $(\lambda_m)_{m \in \mathbb{N} \setminus \{0\}}$ of associated weak eigenvalues such that

$$0 < \lambda_1 \leq \lambda_2 \leq \dots \nearrow \infty.$$

Assume that g is such that the components $G_{i,j}$, $i, j = 1, 2$, of the matrix G satisfy the following properties:

- $G_{i,j}$ is bounded for $i, j = 1, 2$ on Ω_M ;
- there exists $C > 0$ such that $\det G \geq C$ on Ω_M .

A sufficient condition for these assumptions to hold is fulfilled if there exists a compact set K such that $\Omega_M \subset K \subset U$. The assumptions ensure that the integrals in $(\mathcal{W}\mathcal{P})$ exist. Besides, assuming $\Omega := \pi(\Omega_M)$ to have a polygonal boundary is sufficient for the well-definition of all the tools used defined above, in particular to derive the weak formulation $(\mathcal{W}\mathcal{P})$. Note that these assumptions on g and Ω hold in the numerical computations presented in Section 4.

In order to express $(\mathcal{W}\mathcal{P})$ in $(\mathbb{R}^2, (\cdot|\cdot)_G)$ using the chart, let H denote the space $L^2(\Omega)$ equipped with the inner product $(\cdot|\cdot)_H$ given by

$$(v|w)_H = \int_{\Omega} v(\mathbf{x})w(\mathbf{x})\sqrt{\det G(\mathbf{x})} \, d\mathbf{x} \quad \text{for all } v, w \in H,$$

where $\mathbf{x} = (x_1, x_2)$. The assumptions made on g ensure that H is a Hilbert space and that the norm $\|\cdot\|_H$ is equivalent to $\|\cdot\|_{L^2(\Omega)}$. Moreover, this implies that the injection

$$i : (H_0^1(\Omega), (\cdot|\cdot)_{H_0^1(\Omega)}) \hookrightarrow (H, (\cdot|\cdot)_H)$$

is compact, and that $(H_0^1(\Omega), (\cdot|\cdot)_{H_0^1(\Omega)})$ is dense in $(H, (\cdot|\cdot)_H)$. Let a denote the bilinear and symmetric form

$$a : H_0^1(\Omega) \times H_0^1(\Omega) \rightarrow \mathbb{R}, \quad (u, v) \mapsto a(u, v) = \int_{\Omega} \nabla u^T G^{-1} \nabla v \sqrt{\det G},$$

which is continuous and coercive (or $H_0^1(\Omega)$ -elliptic) by assumption on g . The problem $(\mathcal{W}\mathcal{P})$ can be now expressed using the chart as follow:

$$\begin{cases} \text{Find } u \in H_0^1(\Omega_M), u \neq 0, \text{ and } \lambda \in \mathbb{R} \text{ such that} \\ a(u \circ \pi^{-1}, v \circ \pi^{-1}) = \lambda (u \circ \pi^{-1} | v \circ \pi^{-1})_H \text{ for all } v \in H_0^1(\Omega_M). \end{cases} \quad (\mathcal{W}\mathcal{P})$$

Remark 2.1. The relation between the solutions and the weak solutions of (\mathcal{P}) depends on the regularity of $\partial\Omega$. The weak formulation is built on Green's formula, which holds for polygonal (and smoother) domains, so a solution u of (\mathcal{P}) is also a weak solution; see [16, Theorem 1.5.3.1] for the polygonal case. The converse is not always true. It is true for smooth $\partial\Omega$ (see [15, Section 8.4]) as well as for convex polygonal domains and it still holds in some cases for more general polygonal domains; see [16] and [17, Sections 2.1, 2.4]. Thus, it is more consistent to consider subsequently $(\mathcal{W}\mathcal{P})$ instead of (\mathcal{P}) in the optimization problem $(\mathcal{P}_{\text{opt}})$. Indeed, on the first hand, the numerical computations deal with an approximation of the problem $(\mathcal{W}\mathcal{P})$ itself and not directly with (\mathcal{P}) . On the other hand, it cannot be guaranteed that polygonal domains that occur during the optimization process are indeed solutions of (\mathcal{P}) .

2.2 Discretization of the Underlying Problem

A finite element method is used to solve the problem $(\mathcal{W}\mathcal{P})$ numerically. The Galerkin method consists in reformulating it as a *similar* problem in a family of finite dimensional functional subspaces $V_h \subset H_0^1(\Omega)$ associated to a family of meshes \mathcal{M}_h :

$$\begin{cases} \text{Find } u_h \in V_h, u_h \neq 0, \text{ and } \lambda_h \in \mathbb{R} \text{ such that} \\ a(u_h, v_h) = \lambda_h (u_h | v_h)_H \text{ for all } v_h \in V_h. \end{cases} \quad (\mathcal{W}\mathcal{P}_h)$$

Note that because of the regularity of π , $(\mathcal{W}\mathcal{P}_h)$ can be expressed in terms of functions directly defined on Ω . Existence of solutions u_h and λ_h , called respectively *approximated eigenfunctions* and *approximated eigenvalues*, holds thanks to the inclusion $V_h \subset H_0^1(\Omega)$. Combined with the min-max principle and using a similar notation for the sequence of approximated eigenvalues, it implies

$$\lambda_m \leq \lambda_{h,m} \quad \text{for all } m \in \mathbb{N} \setminus \{0\}; \tag{2}$$

see for example [12, Section VI.2]. The subscript h stands for the dependance on the geometry of the mesh, more precisely

$$h := \max_{K \in \mathcal{M}_h} h_K = \max_{K \in \mathcal{M}_h} \text{diam}(K),$$

where K is the geometric element of a finite element (K, Σ, P) of the mesh \mathcal{M}_h . A standard assumption is to ask the family $(\mathcal{M}_h)_h$ to be *regular* in the following sense:

- h approaches 0;
- there exists a constant $\sigma > 0$ such that $\frac{h_K}{\rho_K} \leq \sigma$ for all h and all $K \in \mathcal{M}_h$, where ρ_K denotes the diameter of the largest sphere inscribed in K .

For the numerical computations, we use a conforming finite element method made of triangles of type (1), as defined in [9, p. 47]. It implies

$$V_h = \{v_h : \bar{\Omega} \rightarrow \mathbb{R} \mid v_h|_{\partial\Omega} \equiv 0, v_h|_K \text{ affine for all triangles } K \text{ of the mesh } \mathcal{M}_h\} \quad \text{for all } h.$$

Remark 2.2. A more classical way to discretize a piece of a surface embedded into \mathbb{R}^3 consists in approximating it by a polyhedron having vertices on the surface. That is what is done in [19]. Here, on the contrary, the discretization of the parameter space $\pi(U)$ corresponds to a tessellation of the piece of a surface. Moreover, it allows us to discretize manifolds non-embeddable into \mathbb{R}^3 , like hyperbolic space.

Following the classical process of the finite element method, we introduce a basis $\{\varphi_{h,i}\}_{i=1}^{I_h}$ of V_h , where I_h is the number of nodes $P_i, i = 1, \dots, I_h$, of \mathcal{M}_h inside Ω . With these notations, problem $(\mathcal{W}\mathcal{P}_h)$ consists in solving the finite dimensional eigenproblem

$$S\mathbf{u}_h = \lambda_h M\mathbf{u}_h, \tag{3}$$

where $M, S \in \mathbb{M}_{I_h}(\mathbb{R})$ and $\mathbf{u}_h \in \mathbb{R}^{I_h}$ are given, for all $i, j = 1, \dots, I_h$, by

$$M_{ij} = (\varphi_{h,j} | \varphi_{h,i})_H, \quad S_{ij} = a(\nabla\varphi_{h,j}, \nabla\varphi_{h,i}), \quad \mathbf{u}_{hj} = u_h(P_j).$$

The matrices M and S are symmetric. Moreover, S is positive definite by coercivity of a . This problem is then solved numerically with an Arnoldi/Lanczos process from the ARPACK library; see [21].

Remark 2.3. The integrals appearing in the computation of matrices M and S are approximated using the quadrature formula: both without masslumping (nodes of an element coincide with the middle of its edges) and also for M with masslumping (nodes of an element coincide with the vertices), which makes M to be diagonal. Computations without masslumping provide a numerical value above the exact one according to (2). However, special care is required when using masslumping. In that case some numerical values may be below the theoretical values. It is due to the fact that masslumping may provide only an approximated value of $\lambda_{m,h}$. Unfortunately, the approximated eigenvalue computed with masslumping does not furnish a lower bound for the theoretical eigenvalue in general; see the discussion in [4].

The rest of this subsection is dedicated to a discussion about the estimation of the error made in approximating the weak eigenfunctions u and weak eigenvalues λ by the solutions u_h and λ_h of $(\mathcal{W}\mathcal{P}_h)$. The convergence results need to be distinguished according to the regularity of the weak eigenfunction u of $(\mathcal{W}\mathcal{P})$. By convenience, let us adopt new notations for the rest of this subsection only. Let us denote by $\lambda_{m,1} = \dots = \lambda_{m,q_m} =: \lambda_m$ the m -th weak eigenvalue appearing in $(\mathcal{W}\mathcal{P})$ of multiplicity q_m , and by $u_{m,i}, i = 1, \dots, q_m$, the weak eigenfunctions associated to $\lambda_m, m \in \mathbb{N} \setminus \{0\}$. Moreover, let us denote by E_m the eigenspace associated to λ_m and use a similar notation (with a subscript h) for the approximated eigenvalues, eigenfunctions and eigenspaces of $(\mathcal{W}\mathcal{P}_h)$. Let $h_0(m)$ and $C(m)$ denote two positive constants depending on m .

In the most favorable case, when the weak eigenspaces E_1, \dots, E_m are subsets of $H^2(\Omega)$, there exist $h_0(m)$ and $C(m)$ such that, for all $h < h_0(m)$,

$$\lambda_{h,m} - \lambda_m \leq C(m)h^2.$$

This case arises in particular when Ω is convex or in $\mathcal{C}^{1,1}$; see [18, p. 9]. For a more general domain Ω (such that the spectral theorem holds nevertheless), consider $\Pi_h : H_0^1(\Omega) \rightarrow V_h$ the elliptic projection operator uniquely determined by

$$a(v - \Pi_h v, v_h) = 0 \quad \text{for all } v_h \in V_h.$$

The estimation turns into the following weaker bound for $h < h_0(m)$:

$$\lambda_{h,m} - \lambda_m \leq C(m) \sup_{\substack{v \in \bigoplus_{i=1}^m E_i \\ a(v,v)=1}} \|v - \Pi_h v\|_{H_0^1(\Omega)}^2.$$

Remark 2.4. Actually, the convergence of λ_m depends only on the regularity of the eigenfunctions of the associated eigenspace and not on all the previous eigenfunctions; see [20] for details. Moreover, the following more precise bound can be found in [6, Theorem 3.1]: There exist two positive constants C and h_0 independent of m such that, for $h \leq h_0$,

$$\lambda_{h,m,i} - \lambda_{m,i} \leq C\epsilon_{m,i}(h)^2, \quad i = 1, \dots, q_m, \quad m \in \mathbb{N} \setminus \{0\},$$

where

$$\epsilon_{m,i}(h) := \inf_{\substack{v \in E_m, a(v,v)=1 \\ a(v, u_{h,m,j})=0, j=1, \dots, i-1}} \inf_{v_h \in V_h} a(v - v_h, v - v_h)^{1/2}.$$

With regard to the eigenfunctions, if u_m is simple, then, for h small enough, $u_{h,m}$ is simple, too, and the approximation bound is

$$\|u_{h,m} - u_m\|_{H_0^1(\Omega)} \leq C(m) \sup_{\substack{v \in \bigoplus_{i=1}^m E_i \\ a(v,v)=1}} \|v - \Pi_h v\|_{H_0^1(\Omega)},$$

which, if the weak eigenspaces E_1, \dots, E_m are subsets of $H^2(\Omega)$, turns into

$$\|u_{h,m} - u_m\|_{H_0^1(\Omega)} \leq C(m)h,$$

according to [9, Theorem 3.2.1]. If the multiplicity of λ_m is $\mu \geq 1$, choose the eigenfunctions $u_{m,i}$ such that, for $h \leq h_0$,

$$\|u_{h,m,i} - u_{m,i}\|_{H_0^1(\Omega)} \leq C\epsilon_{m,i}(h),$$

see [6, Theorem 3.1].

3 The Optimization Problem

3.1 Description of the Optimization Problem

The assumptions in the previous section still hold and $m \in \mathbb{N} \setminus \{0\}$ stands for a non-zero integer. Let $(\mathbb{R}^2, (\cdot|\cdot)_G)$ denote abusively the image by π of U in \mathbb{R}^2 endowed with the metric corresponding to g on M , even if π is not onto. In this context, the optimization problem can be reformulated, for a certain fixed volume $0 < V < V_U$, as follows:

$$\left\{ \begin{array}{l} \text{Find a set } \Omega_m^* \subset (\mathbb{R}^2, (\cdot|\cdot)_G) \text{ of induced volume } V \text{ such that the} \\ m\text{-th eigenvalue } \lambda_m \text{ appearing in problem } (\mathcal{W}\mathcal{P}) \text{ satisfies} \\ \lambda_m(\Omega_m^*) \leq \lambda_m(\Omega) \text{ for all sets } \Omega \subset (\mathbb{R}^2, (\cdot|\cdot)_G) \text{ of induced volume } V. \end{array} \right. \quad (\mathcal{P}_{\text{opt}})$$

“Induced” volume means volume measured with G , which is the volume of the corresponding domain in the manifold M . This last formulation of the optimization problem is suitable for the numerical computations.

Remark 3.1. The underlying problem (\mathcal{P}) being now replaced by ($W\mathcal{P}$) in the statement of (\mathcal{P}_{opt}), the scope of this latter problem can be extended to the class of quasi-open sets. In that framework, results from [7, 22] ensure the existence of a bounded solution Ω_m^* .

The main steps of an iteration of the optimization algorithm take place as follows:

- I. establishing a mesh given by the discretization of a boundary;
- II. solving the finite dimensional eigenproblem (3);
- III. moving the boundary nodes of the mesh.

The first step consists only in meshing a domain enclosed by a polygonal curve. At the very beginning of the algorithm, an arbitrary (or guessed) closed curve is given. At the second step, the eigenproblem is solved as explained in the previous section. Finally, the third main step deals with the shape optimization itself. The domain is modified through a displacement of the nodes lying on its boundary. Hence, a new discretization of the boundary is obtained and if a stopping criterion is not reached, the algorithm goes back to step I. The point of this third step is to deform the domain in a *clever* way, in order to get a sequence of domains with increasingly lower associated eigenvalue. It deserves to be described more accurately.

3.2 Details of the Shape Optimization Step

As many methods in the context of shape optimization, a local minimum of a cost functional J is searched using a descent method. In a natural way, the cost functional is given by

$$J : \mathcal{F} \rightarrow \mathbb{R}, \quad \Omega \mapsto J(\Omega) = \lambda_m(\Omega),$$

where \mathcal{F} is the set of all *feasible shapes*. The definition of the set \mathcal{F} comes from [1, Section 6.3]: consider a reference bounded regular open set $\Omega_0 \subset \mathbb{R}^2$ and for $\theta \in W^{1,\infty}(\mathbb{R}^2, \mathbb{R}^2)$ set

$$\mathcal{F} := \mathcal{F}(\Omega_0) = \{\Omega_\theta = (\text{id} + \theta)(\Omega_0)\},$$

where $(\text{id} + \theta)(\Omega_0) = \{x + \theta(x) : x \in \Omega_0\}$. In this way, each feasible shape $\Omega_\theta \in \mathcal{F}(\Omega_0)$ is represented by a *deformation field* $\theta \in W^{1,\infty}(\mathbb{R}^2, \mathbb{R}^2)$. In this context, the variation of the volume and the Hadamard variational formula is given by:

Proposition 3.2 ([13, Corollary 2.1]). *The functional $\text{vol} : \theta \in W^{1,\infty}(\mathbb{R}^2, \mathbb{R}^2) \mapsto \text{vol}(\Omega_\theta) \in \mathbb{R}$ is Fréchet differentiable at $\theta_0 = 0$ with derivative given, for $\theta \in W^{1,\infty}(\mathbb{R}^2, \mathbb{R}^2)$, by*

$$\text{vol}'(\Omega_0)\theta = \int_{\partial\Omega_0} (D\theta(x)|\vec{n}(x))_G \sqrt{\det G(x)} \, d\sigma, \quad (4)$$

where $\vec{n}(x)$ is the outward unit normal (with respect to G) vector on the boundary $\partial\Omega_0$ at the point x , $D\theta(x)$ is the derivative of θ and $d\sigma$ is the corresponding curve element on $\partial\Omega_0$. Moreover if $\lambda_m(\Omega_0)$ is a simple eigenvalue with associated eigenfunction $u_m(\Omega_0)$, the functional $\theta \in W^{1,\infty}(\mathbb{R}^2, \mathbb{R}^2) \mapsto \lambda_m(\Omega_\theta) \in \mathbb{R}$ is Fréchet differentiable at $\theta_0 = 0$ with derivative given, for $\theta \in W^{1,\infty}(\mathbb{R}^2, \mathbb{R}^2)$, by

$$\lambda'_m(\Omega_0)\theta = - \int_{\partial\Omega_0} \left(\frac{\partial u_m(\Omega_0)(x)}{\partial \vec{n}(x)} \right)^2 (D\theta(x)|\vec{n}(x))_G \sqrt{\det G(x)} \, d\sigma. \quad (5)$$

Remark 3.3. The formulas given in the proposition show that only the normal component to $\partial\Omega_0$ of θ affects the derivatives $\text{vol}'(\Omega_0)$ and $\lambda'_m(\Omega_0)$. This fact is specified in [1].

Remark 3.4. It is well known [18, Section 2.5.1] that a multiple eigenvalue is not Fréchet differentiable. To deal with a formula similar to (5) when multiplicity occurs, directional derivatives are used. This is a classical approach in a theoretical context; see [23, Theorem 4.3.1]. However, it does not give a clue about which directional derivative to choose to move the boundary numerically.

Optimization problem $(\mathcal{P}_{\text{opt}})$ can be now addressed. Contrary to the euclidean case [24], the volume constraint must be taken into consideration. Indeed, the functional $\Omega \mapsto \text{vol}(\Omega)\lambda_m(\Omega)$ is in general not invariant by homothety in $(\mathbb{R}^2, (\cdot)_G)$. Thus, the volume of the shape Ω has to be controlled during the optimization process. For this purpose, introduce the Lagrangian \mathcal{L} , given by

$$\mathcal{L} : \mathcal{F}(\Omega_0) \times \mathbb{R} \rightarrow \mathbb{R}, \quad (\Omega, \mu) \mapsto \mathcal{L}(\Omega, \mu) = J(\Omega) + \mu(\text{vol}(\Omega) - V_0),$$

where Ω_0 is an initial shape of volume $0 < V_0 < V_U$, where V_U still denotes the volume of U . The parameter μ is the *Lagrange multiplier* for the problem. The following result transforms $(\mathcal{P}_{\text{opt}})$ into a problem where a saddle point is sought, that is, a point (Ω', μ') satisfying

$$\mathcal{L}(\Omega', \mu) \leq \mathcal{L}(\Omega', \mu') \leq \mathcal{L}(\Omega, \mu') \quad \text{for all } (\Omega, \mu) \in \mathcal{F}(\Omega_0) \times \mathbb{R}. \quad (6)$$

It is a particular case of [10, Theorem 9.3-2].

Lemma 3.5. *With the previous notations, if $(\Omega^*, \mu^*) \in \mathcal{F}(\Omega_0) \times \mathbb{R}$ is a saddle point of the Lagrangian, then the set Ω^* is a solution to problem $(\mathcal{P}_{\text{opt}})$.*

Let us repeat the proof in this context.

Proof. The inequality

$$\mathcal{L}(\Omega^*, \mu) \leq \mathcal{L}(\Omega^*, \mu^*) \quad \text{for all } \mu \in \mathbb{R}$$

in the definition of a saddle point (6) can be rewritten as

$$(\mu - \mu^*)(\text{vol}(\Omega^*) - V_0) \leq 0 \quad \text{for all } \mu \in \mathbb{R},$$

and so, $\text{vol}(\Omega^*) = V_0$. Moreover, the other inequality in (6) yields

$$J(\Omega^*) \leq J(\Omega) + \mu^*(\text{vol}(\Omega) - V_0) \quad \text{for all } \Omega \in \mathcal{F}(\Omega_0),$$

and, restricting to $\Omega \in \mathcal{F}(\Omega_0)$ of volume V_0 , it gives $J(\Omega^*) \leq J(\Omega)$. Thus, Ω^* is a solution of $(\mathcal{P}_{\text{opt}})$. \square

The idea behind the Uzawa algorithm is the following [10]: Assume that the second component $\mu^* \in \mathbb{R}$ of a saddle point of \mathcal{L} is at our disposal. Finding a minimizer Ω^* of the problem (with constraint) $(\mathcal{P}_{\text{opt}})$ is equivalent to finding the first component Ω^* of the saddle point, i.e. a solution to the so-called *primal* problem (without constraint):

$$\begin{cases} \text{Find a set } \Omega^* \in \mathcal{F}(\Omega_0) \text{ such that} \\ \mathcal{L}(\Omega^*, \mu^*) \leq \mathcal{L}(\Omega, \mu^*) \text{ for all } \Omega \in \mathcal{F}(\Omega_0). \end{cases} \quad (\mathcal{P}_{\mu^*})$$

The point is first to be able to find μ^* . It comes readily that μ^* satisfies

$$\inf_{\Omega \in \mathcal{F}(\Omega_0)} \mathcal{L}(\Omega, \mu^*) = \sup_{\mu \in \mathbb{R}} \inf_{\Omega \in \mathcal{F}(\Omega_0)} \mathcal{L}(\Omega, \mu).$$

So, the following *dual* problem has to be solved:

$$\{ \text{Find } \mu^* \in \mathbb{R} \text{ such that } L(\mu^*) = \sup_{\mu \in \mathbb{R}} L(\mu), \quad (\mathcal{Q})$$

where $L : \mathbb{R} \rightarrow \mathbb{R}$ is given by

$$\mu \mapsto L(\mu) = \inf_{\Omega \in \mathcal{F}(\Omega_0)} \mathcal{L}(\Omega, \mu).$$

Thus, to find numerically the solution Ω^* of $(\mathcal{P}_{\text{opt}})$, two sequences $(\Omega^{(n)})_{n \in \mathbb{N}}$ and $(\mu^{(n)})_{n \in \mathbb{N}}$ are built simultaneously using a descent method. For this purpose, the expressions of the Fréchet derivatives of the Lagrangian are required. Their computation comes readily from (4) and (5): for $\Omega \in \mathcal{F}(\Omega_0)$, $\theta \in W^{1,\infty}(\mathbb{R}^2, \mathbb{R}^2)$ and $\mu \in \mathbb{R}$,

$$\frac{\partial \mathcal{L}}{\partial \Omega}(\Omega, \mu)\theta = \int_{\partial \Omega} \left(\mu - \left(\frac{\partial u_k(\Omega)(x)}{\partial \vec{n}(x)} \right)^2 \right) (\theta(x) | \vec{n}(x))_G \sqrt{\det G(x)} \, d\sigma, \quad (7)$$

$$\frac{\partial \mathcal{L}}{\partial \mu}(\Omega, \mu) = \text{vol}(\Omega) - V_0.$$

The initialization of the algorithm consists in an arbitrary Lagrange multiplier $\mu^{(0)} > 0$ and in an arbitrary polygonal domain $\Omega^{(0)}$ of volume V_0 . Then, a typical iteration contains the two following steps:

- (i) Compute $\Omega^{(n+1)}$. To find the infimum of $\Omega \mapsto \mathcal{L}(\Omega, \mu^{(n)})$, we want equation (7) to vanish for all deformation fields θ . Numerically, the domains Ω used are polygonal sets, so the only points controlled are their vertices $P_i^{(n)}$, $i = 1, \dots, N_{\partial\Omega^{(n)}}$. The new position $P_i^{(n+1)}$ of $P_i^{(n)}$ is the point on the line passing through $P_i^{(n)}$ in the direction of $\vec{n}(P_i^{(n)})$ at a distance d_i given by

$$d_i = \int_{\partial\Omega^{(n)}} \left(\mu^{(n)} - \left(\frac{\partial u_k(\Omega^{(n)})(x)}{\partial \vec{n}(\vec{x})} \right)^2 \right) (\theta(x) | \vec{n}(x))_G \sqrt{\det G(x)} \, d\sigma, \quad (8)$$

where $\theta \in W^{1,\infty}(\mathbb{R}^2, \mathbb{R}^2)$ is such that

- $\theta(P_i) = \vec{n}(P_i)$;
 - $\theta(P_j) = 0$ for $j \neq i$.
- (ii) Compute $\mu^{(n+1)}$. To vanish equation (7), the next Lagrange multiplier in the Uzawa algorithm is given by

$$\mu^{(n+1)} = \mu^{(n)} + c(\text{vol}(\Omega^{(n)}) - V_0),$$

where $c > 0$ is a fixed parameter.

- (iii) If a given stopping criterion is not reached, back to step (i).

This optimization process is summarized in the following algorithm.

Uzawa Algorithm

Given $\mu^{(0)} > 0$, $\Omega^{(0)}$ a domain of volume V_0 and tol a threshold.

$n \leftarrow 0$; crit $\leftarrow 2$, tol;

while crit $>$ tol

Compute $\Omega^{(n+1)}$ using a descent method given by (8);

Compute $\mu^{(n+1)} \leftarrow \mu^{(n)} + c(\text{vol}(\Omega^{(n)}) - V_0)$;

update crit;

end

Remark 3.6. The outward unit *normal* vector \vec{n} on the boundary $\partial\Omega$ at a vertex P_i of Ω is defined by generalizing an idea of [14] to surfaces. Besides, the value for the parameter c at step (ii) has been fixed at 1000 after some calibration experiments. Furthermore, the chosen stopping criterion is to ask the ratios

$$\frac{\mathcal{L}(\Omega^{(n+k)}, \mu^{(n+k)}) - \mathcal{L}(\Omega^{(n)}, \mu^{(n)})}{\mathcal{L}(\Omega^{(n)}, \mu^{(n)}), \quad k = 1, \dots, 10,$$

to be all smaller than a certain small tolerance $\epsilon > 0$. Thus, the last ten computed values of the Lagrangian vary *little* compared to the tolerance ϵ . It has been adjusted at $\epsilon = 10^{-6}$. Although the volume is not preserved all along the algorithm, note that the volume of the final domain is very close to V_0 .

4 Computations in Dimension Two

4.1 Surfaces Studied Numerically

As mentioned in the previous sections, the main idea is to use a chart (U, π) of the manifold (M, g) in order to make the numerical computations in the open set $\pi(U) \subset \mathbb{R}^2$ endowed with the corresponding metric. The manifolds (M, g) considered in this article are \mathbb{R}^2 , the sphere \mathbb{S}^2 , the Poincaré disc \mathbb{D}^2 and the upper sheet $H \subset \mathbb{R}^3$ of a hyperboloid.

The canonical representation of \mathbb{R}^2 and \mathbb{D}^2 are chosen. Recall that the metric tensor $G_{\mathbb{D}^2}$ evaluated in a point $(u, v) \in \mathbb{D}^2$ is given by

$$G_{\mathbb{D}^2}(u, v) = \frac{4}{(1 - u^2 - v^2)^2} \text{Id}_2,$$

where Id_2 denotes the 2-by-2 identity matrix. For the sphere, the stereographic map (U, π_N) is used, where $U = \mathbb{S}^2 \setminus \{(0, 0, 1)\}$ and

$$\pi_N : U \rightarrow \mathbb{R}^2, \quad (x, y, z) \mapsto \pi_N(x, y, z) = \frac{1}{1-z}(x, y).$$

The corresponding metric tensor $G_{\mathbb{S}^2}$ evaluated in a point $(u, v) \in \mathbb{R}^2$ is given by

$$G_{\mathbb{S}^2}(u, v) = \frac{4}{(1 + u^2 + v^2)^2} \text{Id}_2.$$

The upper sheet of the hyperboloid $x^2 + y^2 - z^2 = -1$ is parametrized by $(\mathbb{R}_{>0} \times]0, 2\pi[, \alpha)$, where α is given by

$$\alpha^{-1} : \mathbb{R}_{>0} \times]0, 2\pi[\rightarrow \mathbb{R}^3, \quad (r, \theta) \mapsto (r \cos(\theta), r \sin(\theta), \sqrt{1 + r^2}).$$

The corresponding metric tensor G_H induced by the euclidean metric of \mathbb{R}^3 on H and evaluated in a point $(r, \theta) \in \mathbb{R}_{>0} \times]0, 2\pi[$ is given by

$$G_H(r, \theta) = \begin{pmatrix} \frac{1+2r^2}{1+r^2} & 0 \\ 0 & r^2 \end{pmatrix}.$$

4.2 Illustration of Convergences

In this section, two numerical experiments are described. The first one illustrates the convergence of a computed eigenvalue to the exact one using nested meshes of a given domain. The second one concerns the convergence of the optimization method.

To verify numerically that the estimation of the error $e_{h,k} := |\lambda_k - \lambda_{h,k}|$ is of order h^2 as stated at the end of Section 2.2, we shall consider a domain Ω where the exact eigenvalues are known and an exact boundary approximation is possible. Moreover, the eigenfunctions must be in $H^2(\Omega)$, which is the case if Ω is convex as mentioned in that subsection. A mesh refinement is then carried out: each triangle is divided into four similar triangles in order to have nested meshes with smaller and smaller parameter h , so at each refinement, h is halved.

In \mathbb{R}^2 we consider the square $S := [0, 1] \times [0, 1]$. A simple separation of variables shows that the spectrum of S is the set

$$\{(k^2 + l^2)\pi^2 \mid l, k \in \mathbb{N} \setminus \{0\}\}.$$

The experimental error $e_{h,1}$ obtained seems to verify the theoretical result mentioned previously [6, Theorem 3.1] (the slopes in Figure 1 are approximatively equal to 2).

On the sphere, no simple example with exact boundary approximation has been found. However, it is known that the first eigenvalue of $-\Delta_g$ on \mathbb{S}^2 is 2 and that the coordinate functions in \mathbb{R}^3 are associated eigenfunctions; see [8, Section II.4, Proposition 1]. In particular, they have a hemisphere as a nodal domain, and so the first eigenvalue of a hemisphere is also 2, that is,

$$\lambda_1(B_{\pi/2}(\mathbb{S})) = 2,$$

where $B_{\pi/2}(\mathbb{S})$ is the ball centered in $\mathbf{S} = (0, 0, -1)$ of radius $\pi/2$ in \mathbb{S}^2 , namely the southern hemisphere. Notice that the order of convergence in that case is the same, despite of the approximation of the domain. For both examples, the computed error $e_{h,1}$ is represented in Table 1 and in Figure 1.

To illustrate the convergence of the optimization algorithm, we chose the seventh eigenvalue of a domain of volume 0.1 in the Poincaré disc. The motivation to present such an example comes from the need to take the metric into consideration to deal with it. Moreover, the associated optimizing domain is non-symmetric as presented in the sequel.

The method of optimization described in Section 3.1 is based on a descent algorithm, which provides *local* minima. Starting from various initial domains is necessary to enhance the effectiveness of the method to find *global* minima. In this article, only an example leading to the shape having the smallest eigenvalue obtained is given, namely a square. See [25] for a more complete presentation. Its boundary is discretized

h	$e_{h,1}(S)$ with (left) and without (right) masslumping		h	$e_{h,1}(B_{\pi/2}(S))$ with (left) and without (right) masslumping	
$0.2\sqrt{2}/2^2$	-0.164,	0.488	0.492	-0.072,	0.171
$0.2\sqrt{2}/2^3$	-0.041,	0.122	0.253	-0.020,	0.046
$0.2\sqrt{2}/2^4$	-0.010,	0.030	0.135	-0.006,	0.012
$0.2\sqrt{2}/2^5$	-0.003,	0.008	0.0706	-0.002,	0.003
$0.2\sqrt{2}/2^6$	-0.0006,	0.0019	0.0380	-0.0004,	0.0007

Table 1. Error resulting from the approximation of $\lambda_1(S) \approx 19.739$ on nested meshes of the square $S \subset \mathbb{R}^2$ (left) and of $\lambda_1(B_{\pi/2}(S)) = 2$ on nested meshes of the hemisphere $B_{\pi/2}(S) \subset \mathbb{S}^2$ (right).

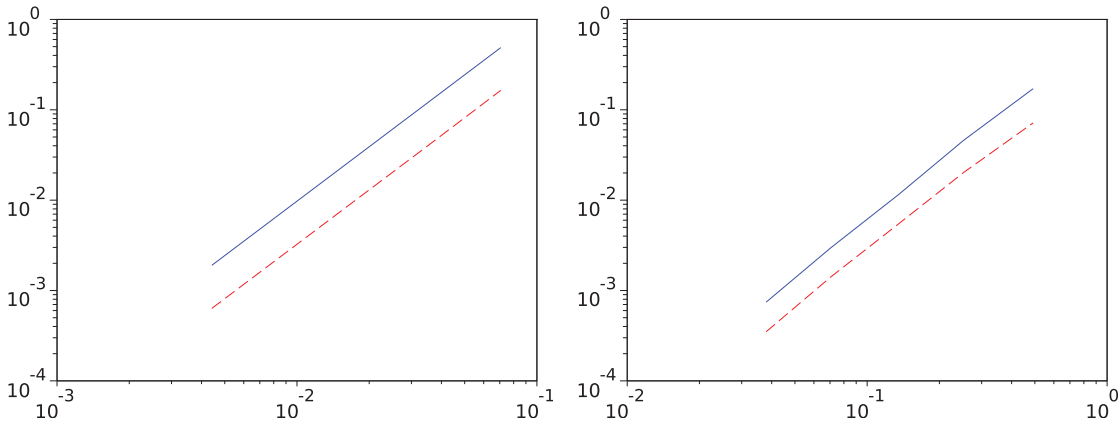


Figure 1. Graph of $h \mapsto e_{h,1}(S)$ (left) and of $h \mapsto e_{h,1}(B_{\pi/2}(S))$ (right) in a logarithmic scale. The blue plain curves correspond to computations without masslumping and the red dashed ones to computations with masslumping.

uniformly using 100 points corresponding to 1250 triangles. Then the optimization algorithm is performed and a candidate to be an optimal domain is obtained. To reach better accuracy, two successive refinements of the mesh are performed similar to those used in the first experiment described in this subsection. Figures 2 and 3 represent the evolution of the Lagrange multiplier during the optimization process, together with the evolution of the volume, the eigenvalue and the value of the cost functional J introduced in Section 3.1. In this example, all these quantities converge relatively quickly, in particular the volume converges to the initial volume as requested by the constraint imposed in the optimization problem. The value of the obtained eigenvalue $\lambda_7^*(\Omega_{7,D^2})$ and the corresponding domain Ω_{7,D^2} are given in Table 3.

4.3 Numerical Investigations

First, the program is run to find the optimizer $\Omega_{k,\mathbb{R}^2}^*$, $k = 1, \dots, 15$, for the fifteen first eigenvalues in \mathbb{R}^2 . Even if the volume constraint is not necessary in this case, the program is used without any modifications to compare the results with [2, p. 13]. The shapes obtained match the ones in [2]. They are presented in Table 2, each eigenvalue being computed with and without masslumping.

Remark 4.1. To reach the optimal domain, the program is started from various initial discretized boundaries. In particular, they have different numbers of connected components. For $\lambda_k(\Omega)$ with $\Omega \subset \mathbb{R}^2$ and $k \geq 2$, it happens that resulting domains are made of connected component realizing the optimum for λ_l with $l < k$. This is related to the result from Wolf and Keller [26, Theorem 8.1]. In spite of the lack of homothety in \mathbb{S}^2 and \mathbb{D}^2 , a similar behavior is noticed in these cases.

Another numerical experiment consists in computing the optimizers for *small* domains in the sphere and in the Poincaré disc. Let $\Omega_{k,\mathbb{S}^2}^*$ and $\Omega_{k,\mathbb{D}^2}^*$ denote the optimizer for the k -th eigenvalue in the sphere and in the Poincaré disc, respectively. A behavior similar to the one observed in \mathbb{R}^2 is expected, that is, optimizing

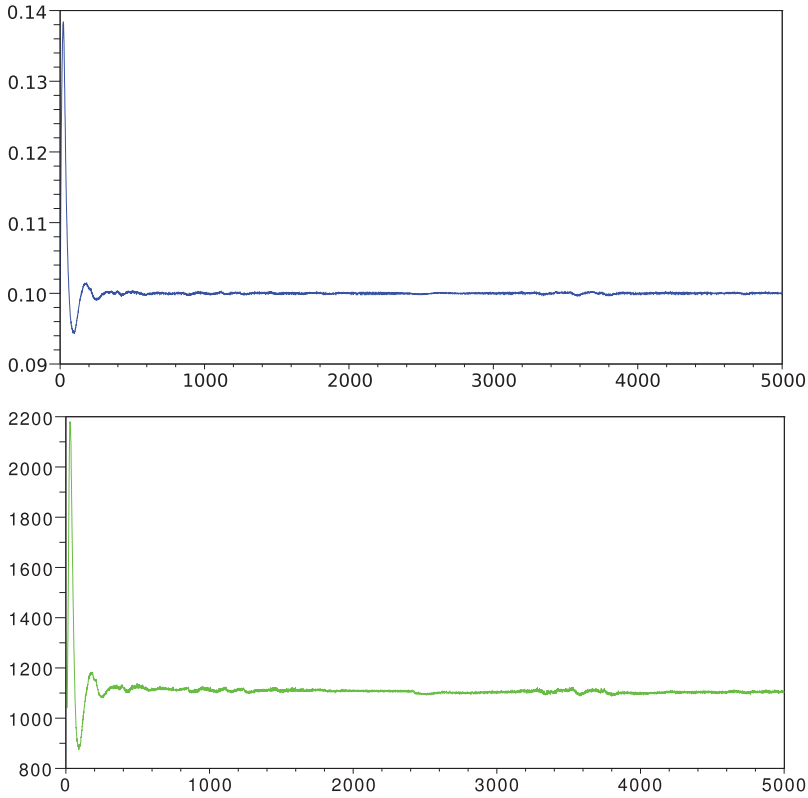


Figure 2. Evolution of the volume of the domain (top) and of the cost functional \mathcal{L} (bottom) with respect to the iteration of the optimization process starting from Ω_s .

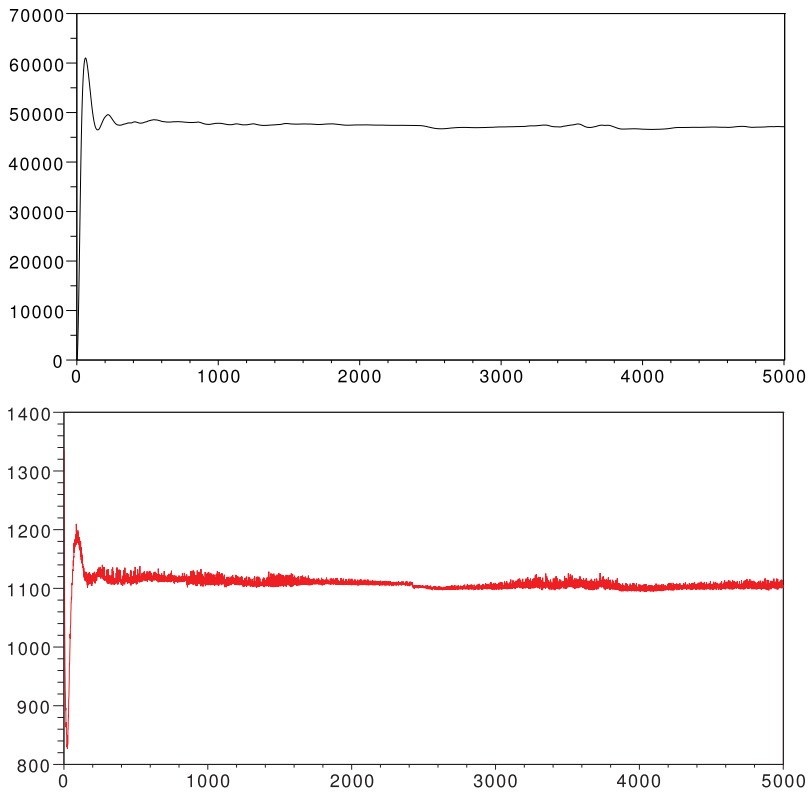


Figure 3. Evolution of the eigenvalue of the domain (top) and of the Lagrange multiplier (bottom) with respect to the iteration of the optimization process starting from Ω_s . The eigenvalue is computed without masslumping.
















k	$\lambda_k(\Omega_{k,\mathbb{R}^2}^*)$ with (left) and without (right) masslumping	$\Omega_{k,\mathbb{R}^2}^*$	$\lambda_k(\tilde{\Omega})$ in [2]
1	18.16, 18.17		–
2	36.32, 36.39		–
3	46.27, 46.30		–
4	64.56, 64.78		–
5	78.46, 78.53		78.2
6	88.89, 89.05		88.52
7	106.40, 106.51		106.14
8	119.84, 120.01		118.9
9	133.71, 134.06		132.68
10	144.39, 144.82		142.72
11	160.32, 160.55		159.39
12	173.97, 174.37		172.85
13	188.47, 188.84		186.97
14	201.64, 202.22		198.96
15	210.65, 211.16		209.63

Table 2. Numerical approximation of $\lambda_k(\Omega_{k,\mathbb{R}^2}^*)$, $k = 1, \dots, 15$, for $\Omega_{k,\mathbb{R}^2}^* \subset \mathbb{R}^2$ the optimizer of volume 1 for the k -th eigenvalue and corresponding shapes. The last column contains the eigenvalues $\lambda_k(\tilde{\Omega})$ from [2].

domains *look like* those found in \mathbb{R}^2 . Such computations have been made with a fixed volume $V_0 = 0.1$; see Table 3. The domains in the Poincaré disc are also exhibited in this table. Visualizing domains in the sphere is not always convenient so only one example is shown here; see Figure 4. All these results confirm the above expectation.

Then the value of the volume V_0 has been increased up to 2 for domains in the sphere and in the Poincaré disc. The relation between $\text{vol}(\Omega_{k,\mathbb{S}^2}^*)$ and $\lambda_k(\Omega_{k,\mathbb{S}^2}^*)$ is exhibited in Figure 5.

Several remarks can be added to the results of these tables. Concerning the domains obtained having two connected components, namely the candidates for the optimizer of the second and the fourth eigenvalue, the ratio between the volume of the connected components has been performed for both in each space \mathbb{R}^2 , the sphere and the Poincaré disc. First for the plane: theoretically, the ratio for the second eigenvalue is 1 by the

k	$\lambda_k(\Omega_{k,\mathbb{S}^2}^*) \subset \mathbb{S}^2$ with (left) and without (right) masslumping	$\lambda_k(\Omega_{k,\mathbb{D}^2}^*) \subset \mathbb{D}^2$ with (left) and without (right) masslumping	$\Omega_{k,\mathbb{D}^2}^*$
1	180.746, 180.855	182.591, 182.639	
2	363.523, 364.356	363.266, 364.827	
3	460.671, 460.927	463.821, 464.068	
4	635.875, 639.377	645.270, 653.612	
5	782.932, 784.251	788.515, 789.829	
6	887.979, 888.975	892.784, 894.214	
7	1062.208, 1063.127	1085.715, 1089.251	
8	1197.243, 1199.235	1199.010, 1207.212	
9	1328.802, 1330.355	1338.065, 1341.360	
10	1437.185, 1439.525	1441.793, 1445.205	
11	1580.123, 1583.765	1622.091, 1632.550	
12	1736.980, 1738.957	1752.412, 1757.700	
13	1886.076, 1890.493	1884.925, 1887.360	
14	1996.383, 1999.437	2019.539, 2026.394	
15	2120.629, 2125.772	2138.361, 2148.878	

Table 3. Numerical approximation of $\lambda_k(\Omega_{k,M}^*)$, $k = 1, \dots, 15$, for $\Omega_{k,M}^*$ the optimizer of volume 0.1 in $M = \mathbb{S}^2$ and \mathbb{D}^2 for the k -th eigenvalue.

Krahn–Szegő theorem. Moreover, if the optimizer for the fourth eigenvalue is the union of two discs, as it seems to be numerically, the ratio is

$$\frac{j_{0,1}^2}{j_{1,1}^2} \approx 0.394,$$

by [11]. Numerically, we found 0.390. Although no such results exist in \mathbb{S}^2 and in the Poincaré disc, due to the non-invariance by homothety of $\Omega \mapsto \text{vol}(\Omega)\lambda_k(\Omega)$ in these spaces, the corresponding ratios are given for comparison. In \mathbb{S}^2 they are about 0.997 and 0.392, respectively, whereas for the Poincaré disc, they are about 0.999 and 0.387.

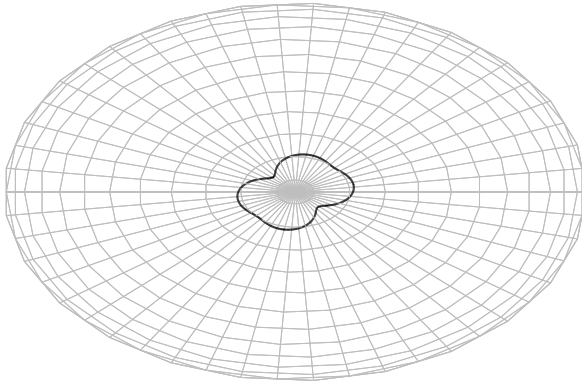


Figure 4. Plot of the optimizer for $\lambda_5(\Omega_{5,\mathbb{S}^2}^*)$ among all domains of volume 0.1 in the sphere \mathbb{S}^2 .

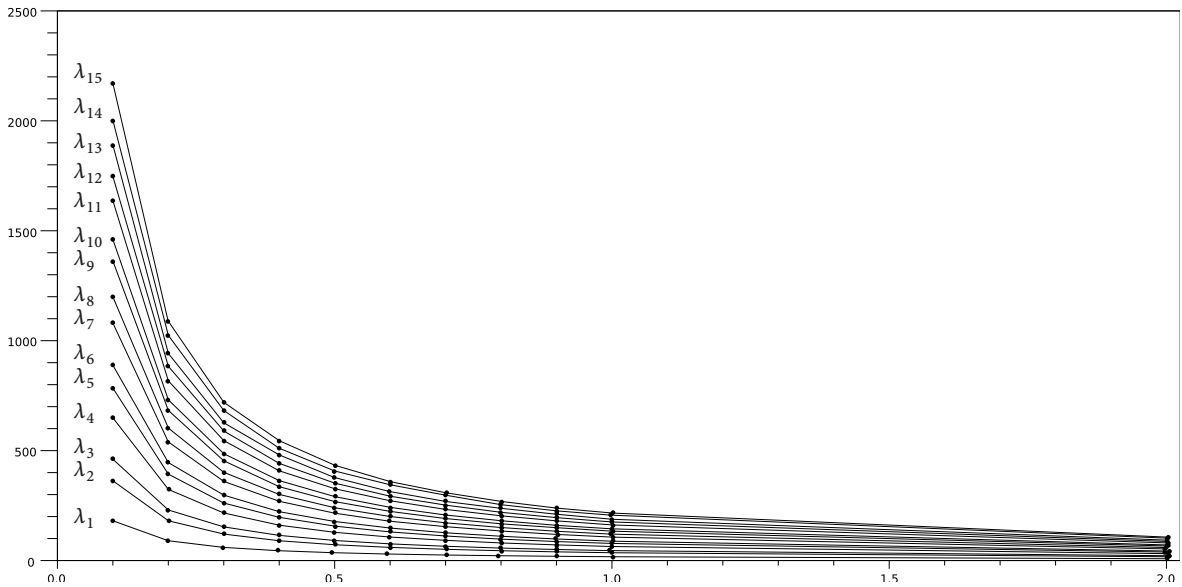


Figure 5. Plot of $\lambda_k(\Omega_{k,\mathbb{S}^2}^*)$ with respect to $\text{vol}(\Omega_{k,\mathbb{S}^2}^*)$ for $k = 1, \dots, 15$.

Besides, another remark is related to the evolution of $\lambda_k(\Omega_{k,E}^*)$, $k = 1, \dots, 15$, with respect to the volume of $\Omega_{k,M}^*$ for the three models $M = \mathbb{R}^2, \mathbb{S}^2, \mathbb{D}^2$. In the plane, this relation is of the form $\lambda_k(\Omega_{k,\mathbb{R}^2}^*) = \text{cst}_k / \text{vol}(\Omega_{k,\mathbb{R}^2}^*)$, $k = 1, \dots, 15$, where cst_k is a positive constant, explicitly known for $k = 1$ and 2 by the Faber–Krahn and the Krahn–Szegő theorems. The corresponding plots for \mathbb{S}^2 are given in Figure 5. In each case, the shape of the optimizer does not change considerably for close volume, as illustrated in Figure 6, for $\lambda_{10}(\Omega_{10,\mathbb{S}^2}^*)$. To compare the three models, see Figure 7 which shows the evolution for the first two eigenvalues. Notice that these eigenvalues decrease less in the Poincaré disc than in \mathbb{R}^2 and in the sphere, where the slope is the deepest.

Finally, some computations in the upper sheet H of the hyperboloid have been performed. The Gaussian curvature of this model is given by

$$\kappa(r, \theta) = \frac{1}{(1 + 2r^2)^2}.$$

In particular, the Gaussian curvature is non-constant, strictly positive and attains its maximum at the point $(0, 0)$ with $\kappa(0, 0) = 1$. Not surprisingly, numerical experiments show that the optimizer $\Omega_{1,H}^*$ for λ_1 is a disc centered at $(0, 0, 1)$. But, although the curvature lies between 0 and 1 in the hyperboloid, this eigenvalue is larger than the first eigenvalue of a ball of same volume in the plane (curvature 0), which is larger than the first eigenvalue of a ball of same volume in the sphere (curvature 1). For instance, denoting by $B_{M,0.01}$ the ball of volume 0.01 in M , it yields numerically

$$\lambda_1(B_{\mathbb{S}^2,0.01}) \approx 1816.57 < \lambda_1(B_{\mathbb{R}^2,0.01}) \approx 1816.80 < \lambda_1(B_{\mathbb{D}^2,0.01}) \approx 1817.67 < \lambda_1(B_{H,0.01}) \approx 1819.10.$$

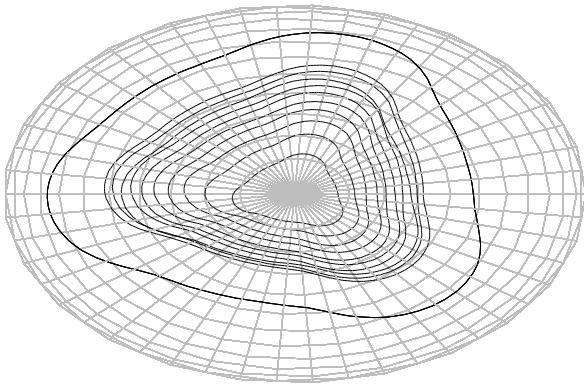


Figure 6. Plot of the optimizers for $\lambda_{10}(\Omega_{10, \mathbb{S}^2}^*)$ and $\text{vol}(\Omega_{10, \mathbb{S}^2}^*) = 0.1, 0.2, \dots, 0.9, 1$ and 2 .

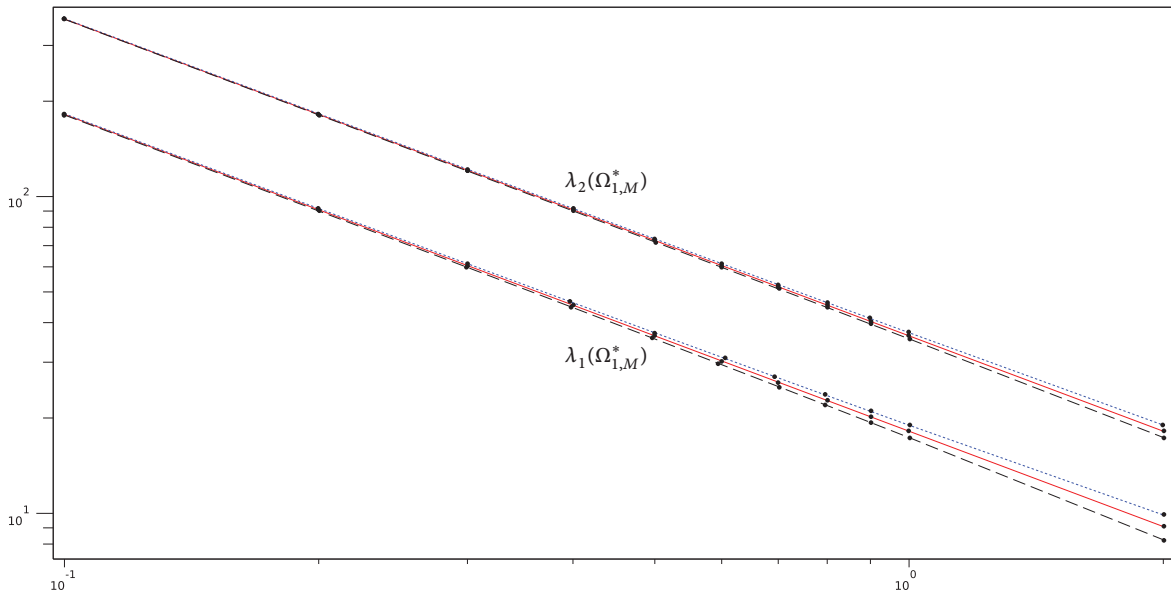


Figure 7. Plot of $\lambda_k(\Omega_{k,M}^*)$ with respect to $\text{vol}(\Omega_{k,M}^*)$ for $k = 1, 2$ and $M = \mathbb{R}^2, \mathbb{S}^2, \mathbb{D}^2$, in a logarithmic scale. The blue dotted curve, the red plain curve and the dashed black curve concern the Poincaré disc, \mathbb{R}^2 and the sphere respectively. The modulus of the slope for the Poincaré disc is less than 1, whereas it is equal to 1 for \mathbb{R}^2 and it is larger than 1 for the sphere.

For the second eigenvalue, the obtained candidate $\Omega_{2,H}^*$ for the optimizer is two discs of same volume, tangent at the point $(0, 0, 1)$. The eigenvalue computed is about 3643.50. So, as for the first eigenvalue, the same ranking with respect to the space occurs for the second eigenvalue.

Since the Gaussian curvature is radial and has its maximum at $(0, 0)$, an optimizer $\Omega_{k,H}^*$ having its center of mass at the origin is expected. The results found for the first two eigenvalues confirm this property. We focused also on the cases $k = 4$ and $k = 13$ since the corresponding optimizers found in the spaces previously studied are not symmetric. Numerically, for a volume equal to 0.1, the candidates for the optimizers are those expected (*same shape* as the corresponding domains found before) and their center of mass are at $(0, 0, 1)$ (actually at a distance of about 10^{-9} of this point); see Figure 8. Looking at the eigenvalues obtained, both $\lambda_4(\Omega_{4,H}^*) \approx 658.329$ and $\lambda_{13}(\Omega_{13,H}^*) \approx 1905.911$ are above the corresponding eigenvalues in \mathbb{R}^2 , in \mathbb{S}^2 and in \mathbb{D}^2 .

In conclusion, the algorithm presented in this article gives the same optimizers in \mathbb{R}^2 as those found previously by the community, and permits to extend the study to other surfaces, even if they do not embed into \mathbb{R}^3 . It can thereby give an intuition in some cases not yet well known theoretically. Thus, some particularities arise quickly because few results exist, as the fact that the eigenvalues of the optimizers for domains in the hyperboloid lie above those in \mathbb{R}^2 and in \mathbb{S}^2 .

Funding: The author was supported by the FNS grant no. 20-137696/1.

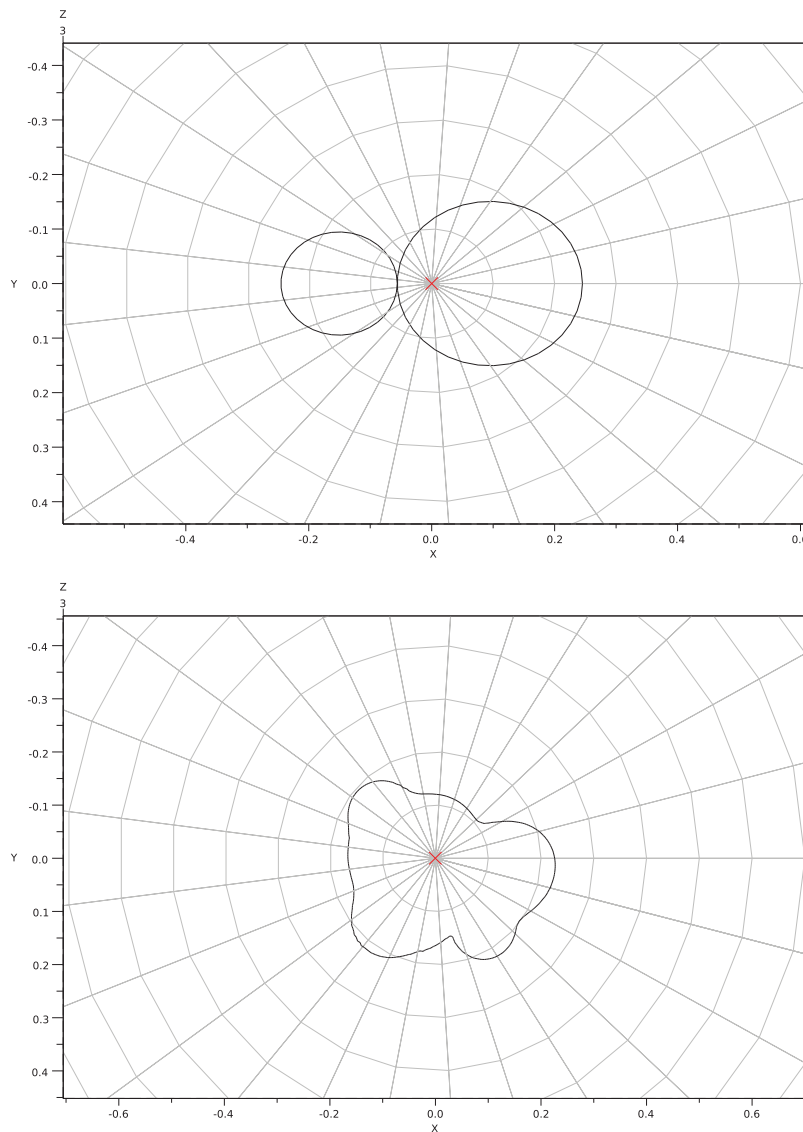


Figure 8. Plot of the optimizers $\Omega_{4,H}^*$ for the fourth eigenvalue (above), and $\Omega_{13,H}^*$ for the thirteenth eigenvalue (below), among all domains of volume 0.1. Their center of mass, indicated by a red cross, lie at the origin.

References

- [1] G. Allaire, *Conception Optimale de Structures*, Math. Appl. (Berlin) 58, Springer, Berlin, 2007.
- [2] P. R. S. Antunes and P. Freitas, Numerical optimization of low eigenvalues of the Dirichlet and Neumann Laplacians, *J. Opt. Theory Appl.* **154** (2012), 235–257.
- [3] P. R. S. Antunes, P. Freitas and J. B. Kennedy, Asymptotic behaviour and numerical approximation of optimal eigenvalues of the Robin Laplacian, *ESAIM Control Optim. Calc. Var.* **19** (2013), 438–459.
- [4] M. G. Armentano and R. G. Durán, Mass-lumping or not mass-lumping for eigenvalue problems, *Numer. Methods Partial Differential Equations* **19** (2003), 653–664.
- [5] M. S. Ashbaugh and R. D. Benguria, Isoperimetric inequalities for eigenvalues of the Laplacian, in: *Spectral Theory and Mathematical Physics: A Festschrift in Honor of Barry Simon's 60th Birthday*, Proc. Sympos. Pure Math. 76, American Mathematical Society, Providence (2007), 105–139.
- [6] I. Babuška and J. E. Osborn, Estimates for the errors in eigenvalue and eigenvector approximation by Galerkin methods, with particular attention to the case of multiple eigenvalues, *SIAM J. Numer. Anal.* **24** (1987), 1249–1276.
- [7] D. Bucur, Minimization of the k -th eigenvalue of the Dirichlet Laplacian, *Arch. Ration. Mech. Anal.* **206** (2012), 1073–1083.
- [8] I. Chavel, *Eigenvalues in Riemannian Geometry*, Pure Appl. Math. 115, Academic Press, Orlando, 1984.

- [9] P. G. Ciarlet, *The Finite Element Method for Elliptic Problems*, Stud. Math. Appl. 4, North-Holland, Amsterdam, 1978.
- [10] P. G. Ciarlet, *Introduction à l'analyse numérique matricielle et à l'optimisation*, Collection Mathématiques Appliquées pour la Maîtrise, Masson, Paris, 1982.
- [11] B. Colbois and A. El Soufi, Extremal eigenvalues of the Laplacian on Euclidean domains and closed surfaces, preprint (2012), hal.archives-ouvertes.fr/docs/00/95/70/58/PS/Extremal-eigenvalues4.ps.
- [12] R. Courant and D. Hilbert, *Methods of Mathematical Physics*, vol. I, Interscience Publishers, New York, 1953.
- [13] A. El Soufi and S. Ilias, Domain deformations and eigenvalues of the Dirichlet Laplacian in a Riemannian manifold, *Illinois J. Math.* **51** (2007), 645–666.
- [14] M. S. Engelman, R. L. Sani and P. M. Gresho, The implementation of normal and/or tangential boundary conditions in finite element codes for incompressible fluid flow, *Internat. J. Numer. Methods Fluids* **2** (1982), 225–238.
- [15] D. Gilbarg and N. S. Trudinger, *Elliptic Partial Differential Equations of Second Order*, Classics Math., Springer, Berlin, 2001. Reprint of the 1998 edition.
- [16] P. Grisvard, *Elliptic Problems in Nonsmooth Domains*, Monogr. Stud. Math. 24, Pitman, Boston, 1985.
- [17] P. Grisvard, *Singularities in Boundary Value Problems*, Recherches en Mathématiques Appliquées 22, Masson, Paris, 1992.
- [18] A. Henrot, *Extremum Problems for Eigenvalues of Elliptic Operators*, Front. Math., Birkhäuser, Basel, 2006.
- [19] M. Jumonji and H. Urakawa, The eigenvalue problems for the Laplacian on compact embedded surfaces and three dimensional bounded domains, *Interdiscip. Inform. Sci.* **14** (2008), 191–223.
- [20] A. V. Knyazev and J. E. Osborn, New a priori FEM error estimates for eigenvalues, *SIAM J. Numer. Anal.* **43** (2006), 2647–2667.
- [21] R. B. Lehoucq, D. C. Sorensen and C. Yang, *ARPACK Users' Guide*, Software, Environments, and Tools 6, SIAM, Philadelphia, 1998.
- [22] D. Mazzoleni and A. Pratelli, Existence of minimizers for spectral problems, *J. Math. Pures Appl. (9)* **100** (2013), 433–453.
- [23] A. Munnier, *Stabilité de liquides en apesanteur, régularité maximale de valeurs propres pour certaines classes d'opérateurs*, Ph.D. thesis, Université de Franche-Comté, 2000.
- [24] É. Oudet, Numerical minimization of eigenmodes of a membrane with respect to the domain, *ESAIM Control Optim. Calc. Var.* **10** (2004), 315–330.
- [25] R. Straubhaar, *Numerical optimization of Dirichlet–Laplace eigenvalues on domains in surfaces*, Ph.D. thesis, University of Neuchâtel, 2013.
- [26] S. A. Wolf and J. B. Keller, Range of the first two eigenvalues of the Laplacian, *Proc. Roy. Soc. London Ser. A* **447** (1994), 397–412.

Received November 5, 2013; revised March 31, 2014; accepted April 2, 2014.